



Version: 1.5

A Study of $Z \rightarrow e^+e^-$ and $Z \rightarrow \mu^+\mu^-$ Events Produced at Low Transverse Momentum Using a Novel Technique

The DØ Collaboration
URL <http://www-d0.fnal.gov>
(Dated: July 31, 2008)

The Z boson transverse momentum, p_T^Z , can be decomposed into two components, a_T and a_L , that are transverse and parallel, respectively, to the di-lepton thrust axis. Using the a_T distribution of Z decays observed with the DØ detector, we measure g_2 , a phenomenological parameter in the BLNY non-perturbative form factor. In a combined measurement with di-muon and di-electron decay channels, using approximately 2 fb^{-1} of data, we measure $g_2 = 0.63 \pm 0.02 \pm 0.04 \text{ GeV}^2$. The first uncertainty is experimental and the second uncertainty is due to the PDF dependence of the theoretical prediction.

Preliminary Results for Summer 2008 Conferences

I. MOTIVATION

The shape of the Z Boson momentum distribution transverse to the beam direction (p_T^Z) at a hadron collider tests the predictions of quantum chromodynamics (QCD), since non-zero p_T^Z is generated through radiation from the initial state partons. A good understanding of electroweak vector boson production is important in precision measurements (e.g., top and W mass).

At low p_T^Z ($p_T^Z \ll Q$, where Q is the mass of the di-lepton system and $Q \approx M_Z$, the Z mass) the emission of multiple soft gluons is important and calculations in fixed order perturbative QCD diverge. There exist resummation techniques, in which contributions from all orders of α_s are resummed to give a finite result. Resummation was first applied to the Drell-Yan process by Collins, Soper and Sterman (CSS) [1]. The resummation is carried out in impact parameter (b) space and includes a non-perturbative (NP) form factor that needs to be determined from data. As discussed in Ref. [2], various forms have been proposed, including the Brock-Landry-Nadolsky-Yuan (BLNY) form:

$$S_{NP}(b, Q^2) = \left[g_1 + g_2 \ln\left(\frac{Q}{2Q_0}\right) + g_1 g_3 \ln(100x_i x_j) \right] b^2, \quad (1)$$

where x_i and x_j are the fractions of the hadron momenta carried by the initial state partons, $Q_0 = 1.6$ GeV is an arbitrary scale and the parameters g_i need to be fitted from data.

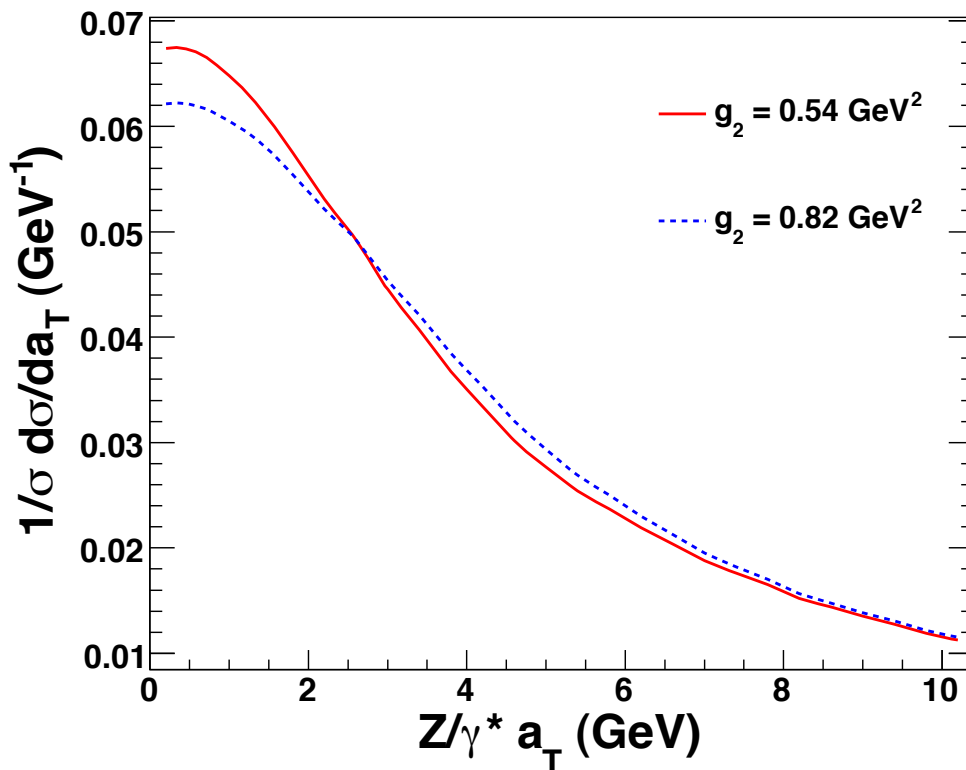


FIG. 1: The normalized a_T distribution for events generated with ResBos [3] for two different g_2 values.

Using the BLNY NP form factor, the CSS formalism was able to describe universally Tevatron Run I Z data and Drell-Yan data from lower Q^2 experiments [2]. The p_T^Z distribution at the Tevatron ($Q^2 \sim M_Z^2$) is sensitive to g_2 and almost completely insensitive to g_1 and g_3 . The CSS formalism is implemented in the Next to Leading Order (NLO) event generator ResBos [3]. Figure 1 shows that as g_2 increases the p_T^Z spectrum predicted by ResBos becomes harder. In addition, the total cross section decreases as g_2 increases. In Run II the DØ Collaboration reported a p_T^Z measurement in the di-electron channel with a 1 fb^{-1} data set [4]. For low p_T^Z ($p_T^Z < 30$ GeV), the DØ data is, within the measurement uncertainties, well described by the BLNY formalism.

At low p_T^Z the quoted uncertainties were dominated by the dependence of the experimental acceptance on the parton distribution functions (PDFs) and the following experimental systematics [4]:

- Unfolding the p_T^Z measurement to account for the resolution in the measurement of the E_T of the electrons.
- Correcting for the p_T^Z dependence of the overall event selection efficiency.

The measurement was $g_2 = 0.77 \pm 0.06 \text{ GeV}^2$ for Run II, which can be compared with an earlier measurement of $g_2 = 0.59 \pm 0.06 \text{ GeV}^2$ from Run I [5]. As a result of the substantial experimental systematic uncertainties, the low p_T^Z region was not much better measured in the 1 fb^{-1} Run II analysis than in the 100 pb^{-1} Run I analysis. An experimental observable that is sensitive to the p_T^Z , but less sensitive to these experimental systematics, would be beneficial.

It should be noted that the Run I and Run II measurements used different PDFs. In addition, the Run I measurement used the Ladinsky, Yuan (LY) parameterization [6] as opposed to the BLNY parameterization, although the term in g_2 is the same and any shift due to changing the terms in g_1 and g_3 is smaller than the uncertainties on these measurements.

II. CONSTRUCTING THE a_T OBSERVABLE

The measured p_T^Z is highly sensitive to the lepton p_T resolution. Our goal is to build an observable that is less sensitive to this resolution, considering the fact that collider detectors generally have far better angular resolution than calorimeter E_T or track p_T resolution.

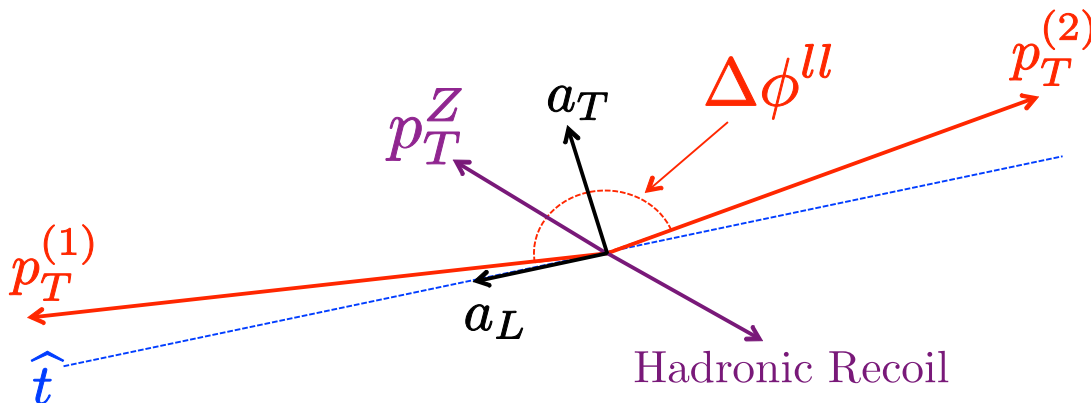


FIG. 2: A schematic representation in the transverse plane, of the construction of a_T and a_L in a typical leptonic Z decay. The hadronic recoil is expected to have equal and opposite p_T to the p_T^Z .

For events with di-lepton azimuthal separation, $\Delta\phi^{\ell\ell} > \frac{\pi}{2}$, the p_T^Z is decomposed into orthogonal components as follows (See Figure 2):

- The event axis is defined as: $\hat{t} = \frac{\vec{p}_T^{(1)} - \vec{p}_T^{(2)}}{|\vec{p}_T^{(1)} - \vec{p}_T^{(2)}|}$ where $\vec{p}_T^{(i)}$ is the transverse momentum vector of lepton i . The two leptons have equal momentum transverse to this axis.
- The transverse momentum of the di-lepton system, $\vec{p}_T^Z = \vec{p}_T^{(1)} + \vec{p}_T^{(2)}$, is decomposed into components transverse to the axis, $a_T = |\vec{p}_T^Z \times \hat{t}|$, and aligned with the axis, $a_L = \vec{p}_T^Z \cdot \hat{t}$.

For events with $\Delta\phi^{\ell\ell} < \frac{\pi}{2}$, a_T is set equal to p_T^Z , while a_L maintains the same definition for all $\Delta\phi^{\ell\ell}$.

At low p_T^Z , $\Delta\phi^{\ell\ell} \sim \pi$, hence the uncertainty on a_T is approximately the same size as the uncertainty on the individual lepton p_T 's multiplied by the sine of a small angle. In contrast, the uncertainty on a_L (and thus also p_T^Z) is approximately the uncertainty on the individual lepton p_T 's multiplied by the cosine of a small angle.

The a_T observable has previously been used in the selection of $\ell^-\ell^+\nu\bar{\nu}$ final states at LEP by the OPAL collaboration [7]. In [8] it has been shown that a_T is almost insensitive to the transverse momentum resolution of the individual leptons. On an event-by-event basis, a_T is therefore more precisely determined than p_T^Z ; this has the consequence that the di-muon channel can be employed in this measurement in addition to the di-electron channel. Furthermore, a measurement of the a_T distribution is demonstrated in [8] to be substantially less sensitive to the dominant experimental systematics (resolution unfolding and dependence of the event selection efficiency on p_T^Z) reported in previous measurements of the p_T^Z .

III. MEASUREMENT STRATEGY

We measure g_2 , the phenomenological parameter used in the BLNY non-perturbative form factor. This is a “detector level” measurement whereby the $Z \rightarrow \ell^- \ell^+$ events from the DØ detector are compared to PYTHIA [9] Monte Carlo (MC) events passed through full GEANT [10] simulation of the detector.

$Z \rightarrow \ell^- \ell^+$ events are generated using ResBos (version 04.24.08pn) for 15 different values of g_2 distributed around the world average (0.68 GeV^2) [2], giving a set of generator level templates. The ResBos grid files are provided by P. Nadolsky [11] for the CTEQ6.6 PDFs [12] and the BLNY NP form factor. The default values are used for g_1 and g_3 ($g_1 = 0.21 \text{ GeV}^2$, $g_3 = -0.6$). PHOTOS [13] (version 2.13) is used for QED radiative corrections. For each ResBos template, we define a two-dimensional PYTHIA/ResBos event weight, binned in generator level p_T^Z and $|y|$. This gives 15 PYTHIA MC templates corresponding to different values of g_2 . Hereafter, unless otherwise stated, “MC” refers to this re-weighted PYTHIA MC.

The g_2 fit is performed as follows:

- Start with 15 MC templates corresponding to different g_2 values.
- The data-vs-MC χ^2 of the a_T distribution is calculated for each template.
- A 2^{nd} order polynomial is fitted to χ^2 as a function of g_2 : $y = a(x - b)^2 + c$.
- The best fit g_2 is then $b \pm a^{-\frac{1}{2}}$ where the uncertainty is statistical ($\Delta\chi^2 = \pm 1$).

Ultimately, an unfolded and acceptance corrected a_T distribution would be of more general interest. This will be the subject of future work. The aim of the current analysis is to demonstrate the experimental power of decomposing the p_T^Z into a_T and a_L components in a “real life” analysis of a large DØ data sample. We do this by extracting a value of g_2 .

IV. THE DØ DETECTOR

The DØ detector has a central-tracking system, consisting of a silicon microstrip tracker (SMT) and a central fiber tracker (CFT), both located within a 2 T superconducting solenoidal magnet, with designs optimized for tracking and vertexing at pseudorapidities $|\eta| < 3$ and $|\eta| < 2.5$, respectively. Central and forward preshower detectors are positioned just outside of the superconducting coil. A liquid-argon and uranium calorimeter has a central section (CC) covering $|\eta|$ up to ≈ 1.1 , and two end calorimeters (EC) that extend coverage to $|\eta| \approx 3.2$ for electrons, with all three housed in separate cryostats. An outer muon system, covering $|\eta| < 2$, consists of a layer of tracking detectors and scintillation trigger counters in front of 1.8 T iron toroids, followed by two similar layers after the toroids. Luminosity is measured using plastic scintillator arrays placed in front of the EC cryostats. The trigger and data acquisition systems are designed to accommodate the high luminosities of Run II.

V. DATA SELECTION

The data used in this analysis were collected between October 2002 and August 2007. After application of data quality criteria, the total integrated luminosity is approximately 2 fb^{-1} . The data set is divided into two intervals with roughly equal integrated luminosity referred to as Run IIa and Run IIb.

Muons must satisfy the following criteria:

- Must be matched to a central track satisfying the following requirements:
 - $p_T > 15 \text{ GeV}$.
 - Must have at least two hits in the SMT and at least one hit in the CFT.
 - The Distance of Closest Approach to the beam spot (DCA) must be less than 0.02 cm.
 - The track fit must have a χ^2/dof less than 4.
- Must be isolated according to the following criteria:
 - $I^{cal} < 2.5 \text{ GeV}$, where $I^{cal} = \sum_{E_T} (0.4) - \sum_{E_T} (0.1)$, and $\sum_{E_T} (\Delta R)$ is the sum of the calorimeter clusters within a cone of $\Delta R = \sqrt{(\Delta\phi)^2 + (\Delta\eta)^2}$.

– $I^{trk} < 2.5$ GeV, where I^{trk} is the sum of the p_T of tracks within a cone of $\Delta R < 0.5$ of the muon.

- Must pass a veto on cosmic ray muons based on timing information.

Di-muon events are selected by requiring two such muons, one of which must have fired one of the single muon triggers.

Electrons must satisfy the following criteria:

- $E_T > 25$ GeV.
- Must be matched to a track with $p_T > 5$ GeV.
- Must be isolated from other activity in the event according to $f_{iso} < 0.15$, where f_{iso} is the isolation variable, defined as:

$$f_{iso} = \frac{\sum_{E_{total}}(\Delta R) - \sum_{E_{EM}}(\Delta R)}{\sum_{E_{EM}}(\Delta R)} \quad (2)$$

where $\sum_{E_{total}}(\Delta R)$ and $\sum_{E_{EM}}(\Delta R)$ are the total and EM calorimeter energies respectively, in a cone of radius ΔR around the electron cluster.

- $f_{EM} > 0.9$, where f_{EM} is the EM fraction defined as:

$$f_{EM} = \frac{E_{EM}}{E_{EM} + E_{Had}} \quad (3)$$

where E_{EM} and E_{Had} are the cluster energies measured in the electromagnetic and hadronic calorimeters respectively.

- The shower shape is required to be consistent with that of an electron.
- The value of a multi-variable likelihood discriminant is required to be consistent with that of an electron.
- Must be in either the central calorimeter (CC) $|\eta| < 1.1$, or one of the end cap calorimeters (EC) $1.5 > |\eta| > 3.2$.
- Must be within the fiducial region of the calorimeter.

Di-electron events are selected by requiring two such electrons. In addition, we require that:

- At least one of the two electrons must be in the central calorimeter (CC).
- Either electron must have fired one of the single electron triggers.

The following additional criteria are applied to both di-muon and di-electron events. The two leptons must have opposite sign charges. The di-lepton invariant mass must be between 70 and 110 GeV. Events with $p_T^Z > 40$ GeV are excluded, since the prediction of ResBos has been shown not to give a good description of the data in that region [4]. The total number of selected events in both channels, after all cuts, is listed in Table I.

TABLE I: Number of events after all selection cuts. For di-electrons the numbers are given separately for events in which both electrons are in CC (CCCC), and in which one electron is in CC and the other in EC (CCEC).

di-muon	di-electron		
	CCCC	CCEC	Total
97393	41029	24713	65742

VI. BACKGROUNDS

Backgrounds from $Z \rightarrow \tau\tau$ are included in the detector level MC event sample compared to the data. Because of the requirement on the di-lepton mass and the tight requirements on lepton identification and isolation, backgrounds from hadrons misidentified as leptons or leptons from the semileptonic decay of heavy quarks within jets are expected to be negligible. The background from cosmic ray muons is found to be negligible.

VII. MC OBJECT CORRECTIONS

Because this measurement is made by comparing uncorrected data with detector-level MC events, it is important that the MC gives a good description of the data in all of the basic variables. The standard MC simulation is known not to match the data in some variables. In order to bring the MC into better agreement with the data, a number of corrections determined using $Z \rightarrow \ell\ell$ events, are applied: smearing of the lepton p_T resolution; correction for the efficiency of the trigger, central tracking and lepton identification; correction of the beam profile.

A measurement based on a_T is very sensitive to angular biases; if there are azimuthal variations in the lepton efficiencies that are poorly described by the MC this can introduce a bias into the measurement. The following additional corrections have been developed specifically for this analysis: correction of the electron identification efficiency and energy scale near to the module boundaries in the CC; correction for the muon identification efficiency near to the octant boundaries separately for the regions $|\eta| < 1$ (central) and $|\eta| > 1$ (forward).

After applying these corrections the quality of data/MC agreement is adequate for the purposes of this analysis. Figures 3, 4 and 5 show the comparison of the data with the MC simulation for a_T , a_L and p_T^Z , respectively. The MC has been re-weighted in p_T^Z and $|y|$ to a g_2 value of 0.63, which is close to the mean value of this measurement. With this value of g_2 the a_T , a_L and p_T^Z distributions are reasonably well described by the MC for both di-muon and di-electron samples.

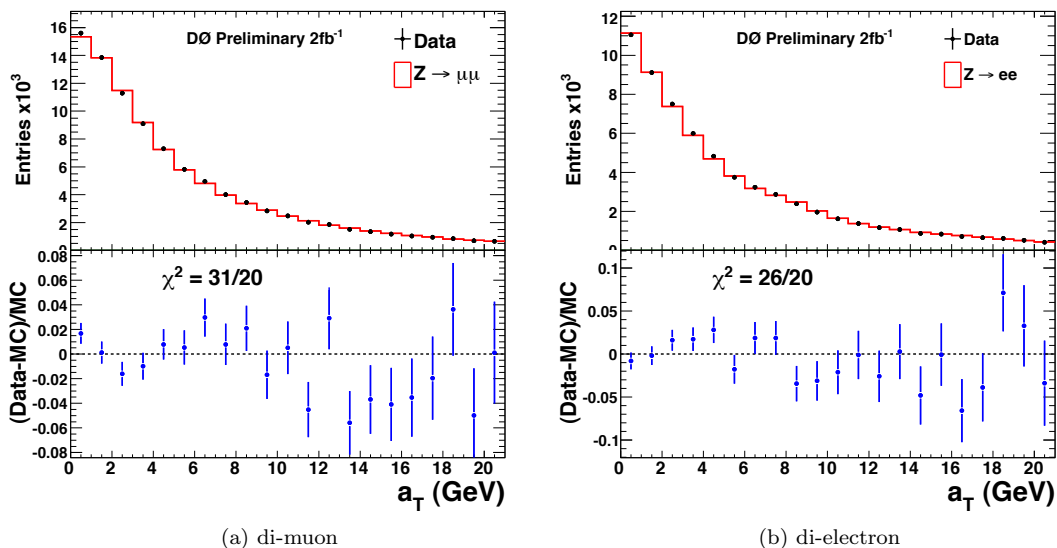


FIG. 3: The a_T distribution for (a) di-muon events, and (b) di-electron events.

VIII. MEASUREMENT OF g_2

In this section, the results of the g_2 measurement and the determination of the systematic uncertainties are presented for the four data samples. Figure 6 shows the χ^2 profiles for g_2 in the four data sets. Table II summarizes the results of the g_2 measurements and the main systematic uncertainties. The following sections detail the evaluation of each systematic uncertainty.

A. Mass window variation

Varying the width of the di-lepton mass window tests the sensitivity to various effects, including backgrounds and asymmetric tails in the lepton p_T resolution. The uncertainty is evaluated by tightening the mass window to [80,100] GeV from the default value of [70,110] GeV. For di-muon events we test the sensitivity to cosmic ray muons by adding the following requirement: $|\eta_{\mu 1} + \eta_{\mu 2}| > 0.02$. The shifts observed in the fitted values of g_2 were +0.002 GeV² in Run IIa and -0.002 GeV² in Run IIb. Averaged over the entire data set the shift is considered to be negligible.

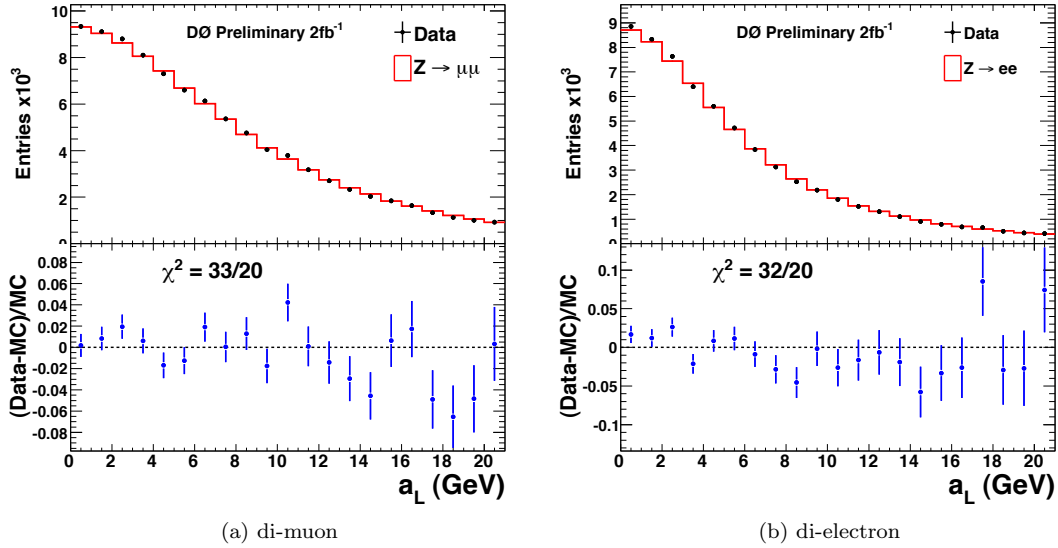


FIG. 4: The a_L distribution for (a) di-muon events, and (b) di-electron events.

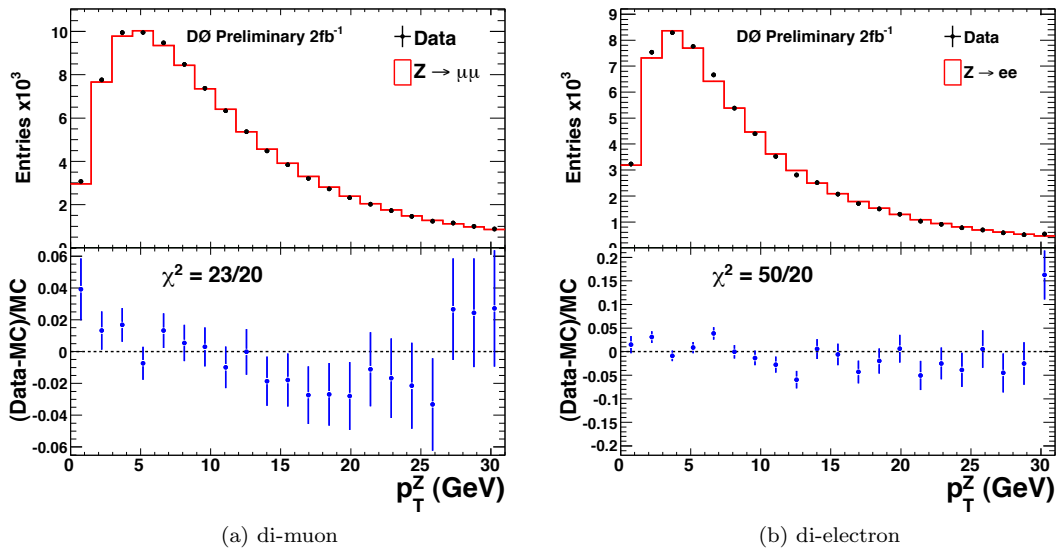


FIG. 5: The p_T^Z distribution for (a) di-muon events, and (b) di-electron events.

TABLE II: Summary of the g_2 measurement and its uncertainties.

	Run IIa $\mu\mu$	Run IIb $\mu\mu$	Run IIa ee	Run IIb ee
Central Value	0.630	0.589	0.656	0.656
Statistical	0.028	0.029	0.030	0.033
Mass window variation	0.015	0.012	0.007	0.009
trigger modeling	0.002	0.002	0.004	0.004
η dependencies	0.004	0.004	0.002	0.002
p_T/E_T smearing	negligible	negligible	negligible	negligible
p_T/E_T scale	0.006	0.006	0.006	0.006
efficiency ϕ dependence	0.010	0.010	0.000	0.018
FSR	0.003	0.004	0.003	0.003
Total uncorrelated	0.034	0.034	0.032	0.039
PDFs	+0.044 -0.034	+0.049 -0.038	+0.035 -0.031	+0.038 -0.034
Total Uncertainty	+0.055 -0.048	+0.060 -0.051	+0.047 -0.045	+0.054 -0.052

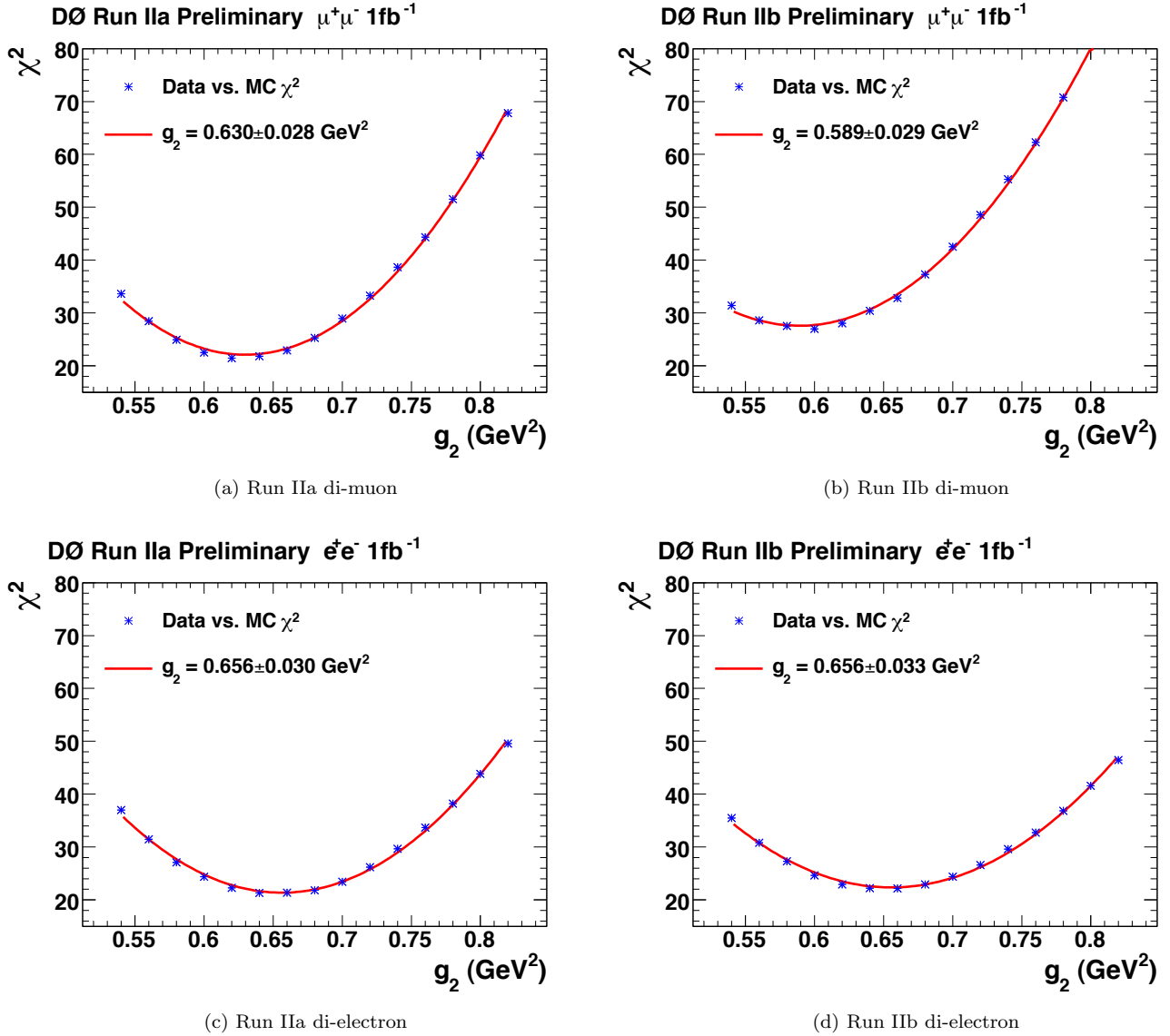


FIG. 6: Data vs MC χ^2 as a function of g_2 for each of the four data sets. The quoted uncertainties are statistical.

B. p_T Turn On Effects

For di-muons, the efficiency in MC is varied by $\pm 10\%$ for $15 < p_T^{\text{muon}} < 20 \text{ GeV}$. For di-electrons, the efficiency in MC is varied by $\pm 10\%$ for $25 < p_T^{\text{electron}} < 30 \text{ GeV}$.

C. η Dependencies

For di-muons, the efficiency in MC is varied by $\pm 10\%$ for $\eta > 1$. For di-electrons, the efficiency in MC is varied by $\pm 10\%$ for $\eta > 1.3$.

D. Electron E_T /Muon p_T Smearing

The smearing of the lepton p_T resolution in the simulation is shifted dramatically, in order to demonstrate the insensitivity of this measurement to any conceivable uncertainty in the smearing parameters. Figure 7 shows the

Run IIa di-electron mass distributions with substantially over- and under-smearred MC. The shift in the fitted g_2 is $+0.5\%$ for over-smearing and -0.1% for under-smearing. For comparison, for a similar fit with p_T^Z , the shift is -38% for over-smearing and $+16\%$ for under-smearing. The systematic uncertainty in a fit with a_T is negligible in both di-muon and di-electron channels.

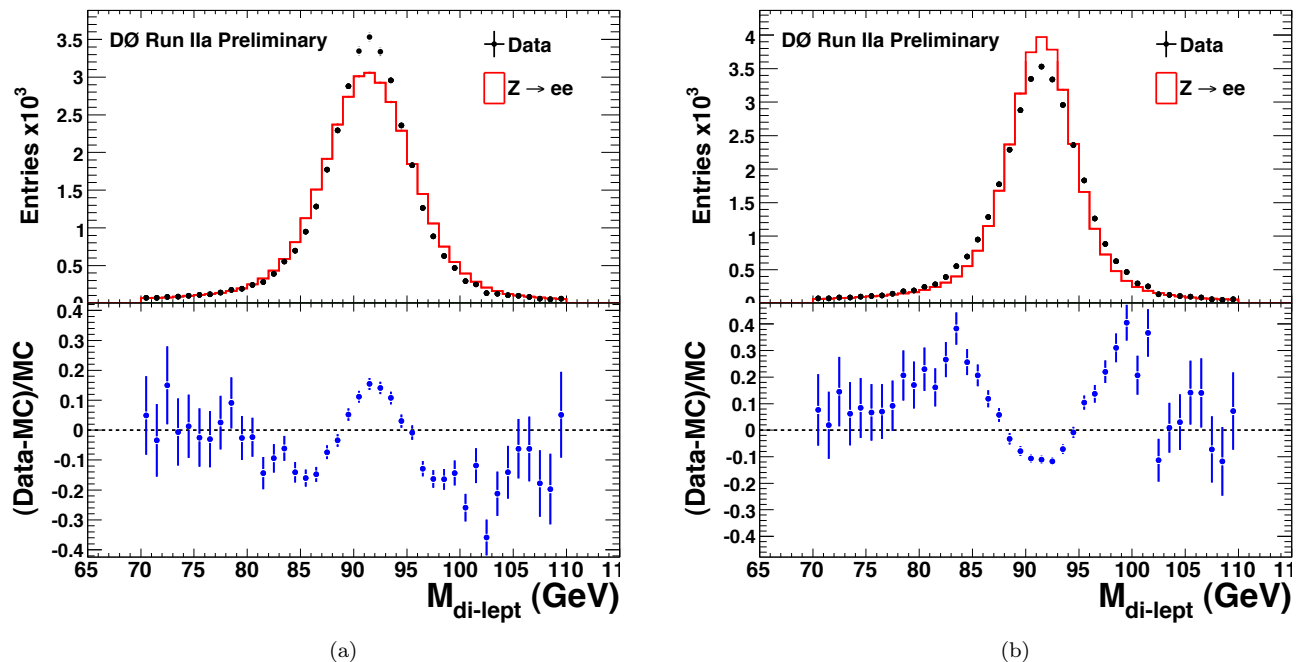


FIG. 7: Distributions of di-electron mass, $M_{di-lept}$, with (a) over-smearred MC and (b) under-smearred MC that nevertheless lead to negligible systematic shifts in the fitted value of g_2 .

E. Lepton Energy/ p_T Scale

In the di-electron channel, the energy scale is shifted by its uncertainty. The muon p_T scale is similarly shifted. Clearly, the a_T distribution is more sensitive to a shift in the energy/ p_T scale than to symmetric resolution effects. However, the resulting systematic uncertainty on g_2 from the considered scale shifts is small.

F. Modeling of the CC Module Boundaries

As a test of the sensitivity to biases from the simulation of electron identification efficiency and energy scale in the region close to the CC module boundaries a number of systematic studies have been carried out; we have found no evidence for any statistically significant deviations. Table III shows the fitted value of g_2 as the width of the fiducial region in the CC is varied. The systematic uncertainty is taken as the shift in g_2 if no fiducial cut is made in the CC.

TABLE III: Fitted g_2 (GeV²) as the width of the fiducial region in the CC is varied (CCCC+CCEC candidates). ϕ^{fract} is the fraction of the azimuthal acceptance in the CC that is removed by the fiducial cut. The default value used in this analysis is $\phi^{fract} = 0.2$.

ϕ^{fract}	g_2 (GeV ²)
0.0	0.648 ± 0.020
0.1	0.642 ± 0.021
0.2	0.656 ± 0.022
0.3	0.659 ± 0.024
0.4	0.633 ± 0.026

G. Muon Octant Boundary Efficiency Correction

If the correction for deficiencies in the MC modeling of the muon identification efficiencies near to the octant boundaries is not applied, the fitted value of g_2 changes by -0.02. We assign 50% of this correction as an uncertainty.

H. Lepton ϕ Resolution

Previous studies using cosmic ray muons have yielded resolutions in ϕ for tracks reconstructed in the central detector in data that are roughly compatible with the MC simulation. Fairly large variations in the ϕ resolution in the MC have been shown to give negligible shifts in the fitted value of g_2 .

I. PDF Uncertainties

The full correlations among g_1 , g_2 , g_3 , and the PDFs will become apparent only through a global fit over all Q^2 . Likewise, a complete analysis of the theoretical uncertainties among them await this fuller phenomenological treatment. For this particular measurement, we can explore the uncorrelated sensitivity of g_2 to PDFs at $Q^2 = M_Z^2$ by simply varying the PDF sets according to their published uncertainties and re-fitting for g_2 . This we characterize as the ‘‘PDF uncertainty’’.

The ResBos events are generated with CTEQ6.6 PDFs [12]. The PDFs are functions of 22 nearly orthogonal parameters. In order to estimate systematic uncertainties due to the PDFs, an additional 44 ‘‘error’’ PDF sets are provided. Each of these corresponds to the upper or lower boundary of the 90% confidence level (CL) interval for one of the 22 parameters. Events are generated using ResBos with each of the error PDF sets, giving 44 templates in p_T^Z and $|y|$. Event weights relative to the central set, binned in p_T^Z and $|y|$, are evaluated for each of the 44 templates and applied to the fully simulated PYTHIA MC event sample. The g_2 measurement is repeated with the event weights corresponding to each PDF error set and the associated uncertainty on g_2 is then given by [12]:

$$\Delta X^\pm = \sqrt{\sum_{i=1}^n (X^\pm - X^0)^2}$$

where X^\pm are the maximum variations in the positive and negative directions for each parameter. The PDF uncertainty is very highly correlated between the di-muon and di-electron analyses. Table IV compares the uncertainties for CTEQ6.1m [14] and CTEQ6.6 PDFs. It should be noted that the central value obtained in the fit using CTEQ6.1m PDFs is about 0.02 GeV² larger than that obtained using CTEQ6.6.

TABLE IV: PDF uncertainties on g_2 evaluated for the CTEQ6.1m and CTEQ6.6 PDF sets.

PDF set	Run IIa $\mu\mu$	Run IIb $\mu\mu$	Run IIa ee	Run IIb ee
CTEQ6.6	+0.044	+0.049	+0.035	+0.038
	-0.034	-0.038	-0.031	-0.034
CTEQ6.1m	+0.034	+0.037	+0.030	+0.033
	-0.041	-0.045	-0.038	-0.041

J. Final State Radiation

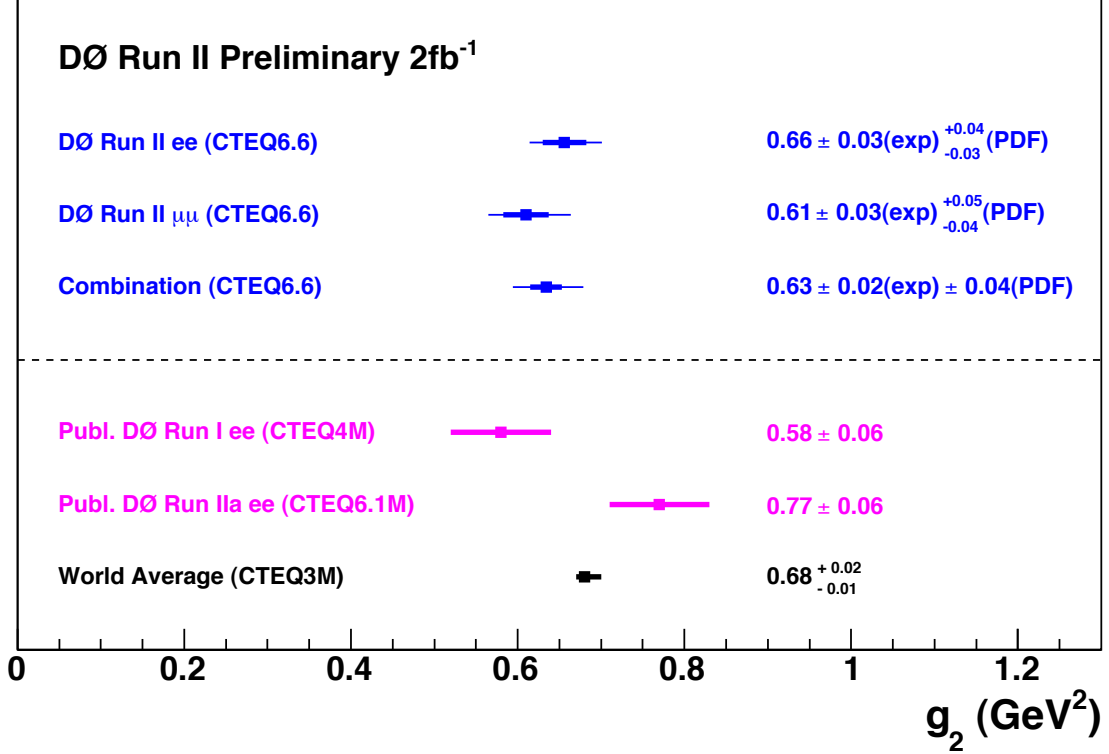
As a estimate of the systematic uncertainty due to final state radiation (FSR), the number of MC events containing a photon that reduces the di-lepton mass by 0.5 GeV or more are scaled up and down by 20%. (PYTHIA MC events contain approximately 20% more such photons than ResBos+PHOTOS events.) The changes in the fitted g_2 are presented in Table V. Given that the changes are roughly symmetric, we assign a symmetric uncertainty of the larger of the two changes.

IX. FINAL g_2 COMBINATION

In combining the four measurements, the PDF uncertainty is treated as 100% correlated between the four measurements. All other systematic uncertainties are treated as uncorrelated between the two channels, but 100% correlated

TABLE V: Change in the fitted g_2 after re-weighting events containing an FSR photon.

weight	Run IIa $\mu\mu$	Run IIb $\mu\mu$	Run IIa ee	Run IIb ee
+20%	-0.003	-0.004	-0.003	-0.003
-20%	+0.002	+0.003	+0.002	+0.003

FIG. 8: Comparison of our g_2 measurement (blue) with previous DØ measurements (purple) and the world average (black). The theoretical uncertainty due to the PDFs is marked by the thinner line (only on the measurements in this analysis).

between Run IIa and Run IIb data sets within the same channel. Measurements in the di-muon and di-electron channels obtained by combining the Run IIa and Run IIb results are given in Table VI and Figure 8. The di-muon and di-electron measurements differ by 1.2σ . Combining the di-muon and di-electron measurements, the final results is $g_2 = 0.63 \pm 0.02 \pm 0.04 \text{ GeV}^2$, where the first uncertainty is experimental and the second is the PDF uncertainty. The results are compared in Figure 8 to previous measurements. Since the world average measurement does not include a PDF uncertainty, we present our measurements with a separate PDF uncertainty.

TABLE VI: Combined Run IIa and Run IIb measurements for each channel with uncertainties.

	Di-muon	Di-electron
Central Value	0.610	0.656
σ_{stat}	0.021	0.022
σ_{syst}	0.018	0.014
$\sigma_{total}(\text{excl. PDF})$	0.028	0.026

X. CONCLUSIONS

Using a data set corresponding to approximately 2 fb^{-1} the parameter g_2 of the BLNY non-perturbative form factor is measured in $Z \rightarrow \ell^- \ell^+$ events from the DØ experiment in both the di-electron and di-muon channels. The combined measurement is; $g_2 = 0.63 \pm 0.02 \pm 0.04 \text{ GeV}^2$. The first uncertainty is experimental and the second uncertainty is the PDF dependence of the theoretical prediction. It should be noted that the PDF uncertainty is 90% CL as opposed to 1σ . None of the previous measurements quote a theoretical PDF uncertainty and this needs to be considered when comparing them to our measurement.

This is the first time that the variable a_T has been used to study the p_T distribution of Z bosons. This technique has allowed a significant reduction in the dominant experimental systematics encountered in previous measurements of the p_T^Z at the Tevatron. In particular, the feature that a_T is insensitive to lepton p_T mis-measurement allows a similarly precise measurement to be made in the di-electron and di-muon channels. Previous measurements of the p_T^Z distribution at the Tevatron [4, 5, 15, 16] have been limited to the di-electron channel. The analysis benefits from the different experimental systematics for the di-muon and di-electron channels.

-
- [1] J. Collins, D. Soper, G. Sterman, Nucl. Phys. B259 (1985) 199.
 - [2] F. Landry *et al.*, Phys. Rev. D 67, 073016 (2003).
 - [3] C. Balazs and C.P.Yuan, Phys. Rev. D 56, 5558 (1997).
 - [4] DØ Collaboration, Phys. Rev. L. 100, 102002 (2008).
 - [5] DØ collaboration, B. Abbott *et al.*, Phys. Rev. D 61, 032004 (2000); DØ collaboration, B. Abbott *et al.*, Phys. Rev. Lett., 84, 2792 (2000).
 - [6] G.A. Ladinsky, C.P. Yuan, Phys. Rev. 50 4239 (1994).
 - [7] OPAL Collaboration, K. Ackerstaff *et al.* Eur. Phys. J C4 47 (1998).
 - [8] M. Vesterinen and T. R. Wyatt, “A Novel Technique for Studying the Z Boson Transverse Momentum Distribution at Hadron Colliders”, arXiv:0807.4956 [hep-ph] 2008 (submitted to Nucl. Instr. and Methods in Phys. Res. **A**).
 - [9] T. Sjöstrand *et al.*, Comput. Phys. Commun. 135, 238 (2001).
 - [10] S. Agostinelli *et al.*, Nucl. Inst. and Methods in Phys. Res. **A 506** 250 (2003).
 - [11] ResBos grid files for the CTEQ6.6 PDFs and BLNY NP form factor are available from the following location: http://hep.pa.msu.edu/resum/grids/resbos_p/w_z/tev2/general_purpose/z0/
 - [12] P. Nadolsky *et al.*, arXiv:0802.0007v3 [hep-ph], 2008.
 - [13] E. Barberio *et al.*, Comput.Phys.Commun. 66 115, (1991).
 - [14] J. Pumplin *et al.*, JHEP 0207 012 (2002); D. Stump *et al.*, JHEP 0310 046 (2003).
 - [15] CDF Collaboration, T. Affolder *et al.*, Phys. Rev. Lett. 84, 845 (2000).
 - [16] CDF Collaboration, T. Aaltonen, *et al*, Phys. Rev. Lett. 100, 102001 (2008).